Dynamic chromosomal rearrangements in Hodgkin's lymphoma are due to ongoing three-dimensional nuclear remodeling and breakage-bridge-fusion cycles

Amanda Guffei,[1] Rahul Sarkar,[1,2] Ludger Klewes,[1] Christiaan Righolt,[1,3] Hans Knecht,[1,4]* and Sabine Mai[1]*

[1]Manitoba Institute of Cell Biology, University of Manitoba, CancerCare Manitoba, Winnipeg, MB, Canada; [2]Department of Medical Biophysics, University of Toronto, ON, Canada; [3]Quantitative Imaging Group, Delft University of Technology, Delft, The Netherlands, and [4]Division of Haematology/Oncology, Department of Medicine, CHUS, University of Sherbrooke, QC, Canada

ABSTRACT

Background

Hodgkin's lymphoma is characterized by the presence of mono-nucleated Hodgkin cells and bi- to multi-nucleated Reed-Sternberg cells. We have recently shown telomere dysfunction and aberrant synchronous/asynchronous cell divisions during the transition of Hodgkin cells to Reed-Sternberg cells.[1]

Design and Methods

To determine whether overall changes in nuclear architecture affect genomic instability during the transition of Hodgkin cells to Reed-Sternberg cells, we investigated the nuclear organization of chromosomes in these cells.

Results

Three-dimensional fluorescent *in situ* hybridization revealed irregular nuclear positioning of individual chromosomes in Hodgkin cells and, more so, in Reed-Sternberg cells. We characterized an increasingly unequal distribution of chromosomes as mono-nucleated cells became multi-nucleated cells, some of which also contained chromosome-poor 'ghost' cell nuclei. Measurements of nuclear chromosome positions suggested chromosome overlaps in both types of cells. Spectral karyotyping then revealed both aneuploidy and complex chromosomal rearrangements: multiple breakage-bridge-fusion cycles were at the origin of the multiple rearranged chromosomes. This conclusion was challenged by super resolution three-dimensional structured illumination imaging of Hodgkin and Reed-Sternberg nuclei. Three-dimensional super resolution microscopy data documented inter-nuclear DNA bridges in multi-nucleated cells but not in mono-nucleated cells. These bridges consisted of chromatids and chromosomes shared by two Reed-Sternberg nuclei. The complexity of chromosomal rearrangements increased as Hodgkin cells developed into multi-nucleated cells, thus indicating tumor progression and evolution in Hodgkin's lymphoma, with Reed-Sternberg cells representing the highest complexity in chromosomal rearrangements in this disease.

Conclusions

This is the first study to demonstrate nuclear remodeling and associated genomic instability leading to the generation of Reed-Sternberg cells of Hodgkin's lymphoma. We defined nuclear remodeling as a key feature of Hodgkin's lymphoma, highlighting the relevance of nuclear architecture in cancer.

Key words: 3D nucleus, chromosomal rearrangements, SKY, 3D-SIM, BBF-cycles, Reed-Sternberg cells.

Introduction

Hodgkin's lymphoma is a malignant post-germinal center derived B-cell lymphoma characterized by the presence of mononuclear Hodgkin cells (H cells) and diagnostic bi- to multi-nuclear Reed-Sternberg cells (RS cells).[2] In 40-50% of cases, H and RS cells express the Epstein-Barr virus encoded oncoprotein LMP1 or its deletion variants.[3,4] As a particularity, circulating small clonotypic precursors are very rare or undetectable,[5] and H and RS cells make up less than 5% of the total cellular mass within the affected lymph nodes, which are composed mainly of reactive T cells.[6] In approximately 85% of patients chemotherapy and autologous bone marrow transplantation result in long-lasting remissions or cure but about 15% of patients still succumb to multiple relapses or have primary resistant disease.[7]

Genomic instability is a hallmark of tumor cells.[8] Different pathways lead to such instability, but, in the context of HL, telomere dysfunction is a prime mechanism leading to the transition of H to RS cells.[1,9,10] As first shown by Müller[11] and McClintock,[12,13] chromosomal end-to-end fusions create dicentric chromosomes that form anaphase bridges and break upon completion of a cell division cycle. After completion of cell division, both daughter cells remain with two 'broken' chromosome ends that represent a double-strand break. In such a breakage-bridge-fusion (BBF) cycle, one daughter cell inherits a terminal deletion and the other one an unbalanced translocation. Such chromosomes are highly reactive, *i.e.* available for rearrangements, including new fusions with additional chromosome ends. Therefore, after one BBF event, both daughter cells are at the origin of divergent clonal evolution and will continue to develop different genetic aberrations when their broken ends fuse with new chromosome partners.[10] This difference in rearrangements is at the origin of chromosomal evolution seen in many complex tumors that exhibit dynamic BBF cycles, such as osteosarcoma, and prostate, breast and colon cancer.[14-21]

Aberrations in centrosome duplication cycles leading to centrosome amplification have been observed in many different cancers[22,23] and are another characteristic feature of RS cells.[1,24-26]

Thus due to the combination of telomere dysfunction, centrosome amplification and defective spindle formation, RS cells are expected to gain increasingly complex karyotypes with respect to their chromosome numbers, rearrangements and nuclear distribution among individual sub-nuclei of the multi-nucleated RS cell. The current study was, therefore, initiated to investigate the dynamics and mechanisms of chromosomal evolution in Hodgkin's lymphoma. Special emphasis was given to the transition of the H to the RS cell. Super resolution microscopy (3D-SIM) was used for the first time to aid the interpretation of mechanisms leading to karyotype evolution in RS cells.

Design and Methods

Cell cultures

L-428, L-1236, and HDLM-2 cell lines, whose origins were described by Knecht *et al.*,[1] were grown in RPMI-1640 medium containing 20% fetal bovine serum, 1% L-glutamine, and 1% penicillin-streptomycin (all reagents were purchased from Invitrogen/Gibco, Burlington, ON,

Canada). Cells were incubated at 37°C with 5% CO_2 for 4 days (1-2 mL of fresh medium was added every second day) until confluent.

Metaphase and interphase fixation

Metaphase chromosomes and 3D nuclei for interphase analysis were prepared as previously described.[27] Three independent experiments were carried out for all three cell lines.

Fluorescent *in situ* hybridization of metaphases and interphases

Whole chromosome paints (Applied Spectral Imaging, Vista, CA, USA) were used to identify chromosome 9 (cyanine 3) and chromosome 22 (flourescein isothiocyanate). Metaphases were dropped onto the slides. Interphase nuclei were maintained using a three-dimensional (3D) fixation protocol[27] and then gently placed onto slides so as not to disrupt the cell structure. Fluorescent *in situ* hybridization (FISH) was carried out as described elsewhere.[28]

Twenty metaphases for each of the cell lines were imaged and 30 multi- and 30 mono-nucleated interphases cells were captured. For each interphase cell, a z-stack of 120 slices was obtained, each at a sampling distance of *xy*: 102 nm and *z*: 200nm. Axiovision 4.5 software (Carl Zeiss, Toronto, ON, Canada) and a constrained iterative algorithm were used for deconvolution.[29] ChromoAnalyze software (see, quantitative analysis of chromosomal overlaps) was used to determine the presence of translocations in the interphases cells. The metaphases were scored visually for abnormalities. All FISH experiments were repeated three times. All results were analyzed statistically.

Quantitative analysis of chromosomal overlaps

In order to detect translocations in both multi-nucleated and mono-nucleated cells, an in-house software tool named ChromoAnalyze, was developed for semi-automated quantitative image analysis. The software was developed using Matlab (The MathWorks, Natick, MA, USA) and employs the DIPLib image processing toolbox (Delft, The Netherlands, *http://www.diplib.org/*). Labeled chromosomes and the nuclear boundary are segmented from their respective fluorescent channels using an iterative intensity thresholding algorithm.[30] Chromosome channel signals outside the segmented nuclear volume are attributed to non-specific signals and thus excluded from analysis. Overlapping chromosome regions are obtained from the logical intersection of the segmented binary images from the fluorescein isothiocyanate- and cyanine 3-labeled chromosome signals.

To facilitate semi-automated analysis by a trained user, an interface that allowed full volumetric rotation and zooming was developed to visualize semi-transparent surface renderings of the two chromosome channels (*Online Supplementary Figure S1A*) and the resulting segmented overlap images in three-dimensions (*Online Supplementary Figure S1B*). Resolution limitations in the imaging system may result in the appearance of "false overlaps", which may lead to: (i) erroneous detection of a translocation when chromosome regions are simply in close proximity; or (ii) misclassification of two spatially-adjacent translocations as a single larger translocation. To correct for the first case, a training set of ten representative nuclei were used to calibrate a parameter that defined the smallest overlapping region corresponding to a translocation. This parameter (≤

5% overlap) was applied in subsequent measurements to exclude small overlaps that were not likely to represent translocations (*Online Supplementary Figure S1C*). For the second case, the interface allowed the user to visually identify and separate two spatially-adjacent translocations that were detected as a single translocation.

Spectral karyotyping

Spectral karyotyping (SKY) was performed using the SKY kit for human chromosomes (Applied Spectral Imaging, Vista, CA, USA) and following the manufacturer's protocol. Slides were imaged using an Axioplan 2 microscope with a 63x/1.4 oil objective (Carl Zeiss, Inc. Canada) and analyzed using Case Data Manager 4.0 software (Applied Spectral Imaging, Vista, CA, USA). Twenty metaphases were imaged and analyzed for all cell lines. Rearrangements were scored and statistically analyzed.

Peptide nuclei acid fluorescence in situ hybridization

Peptide nucleic acid (cyanine 3) FISH was performed on metaphases as described previously.[31] The slides were imaged on an Axioplan 2 microscope with a 63x/1.4 oil objective, using the Axiovision 4.6 software (Carl Zeiss, Inc. Canada). We randomly choose 20 metaphases to image for each cell line. Metaphases were scored by eye and analyzed statistically for aberrations.

Super resolution microscopy

Three-dimensional telomere quantitative FISH (3D-Q-FISH) was performed as described previously.[1] Super resolution microscopy (3D-SIM) image acquisition was performed using an Axio Observer Z1 and a Plan-Apochromat objective 63x/1.4 (both Carl Zeiss, Thornwood, NY, USA) and exposure times of 100 ms (cyanine 3) and 200 ms (4',6-diamidino-2-phenylindole). For 4',6-diamidino-2-phenylindole, we used band pass filters of 420-480nm, while for cyanine 3, we used 570 - 640 nm, and 405 nm and 561 nm lasers for excitation. The software is a beta version of ZEN 2010 (Carl Zeiss, Thornwood, NY, USA). Sampling sizes were x,y: 40 nm and z: 125 nm.

Statistics

Experimental results from FISH, SKY and 3D-Q-FISH were analyzed with Fisher's exact test to determine significant differences between various findings among the data sets. A *P* value of less than 0.05 was considered statistically significant.[9]

Results

Nuclear chromosome organization in Hodgkin and Reed-Sternberg cells

Our previous work on Hodgkin's lymphoma led to the following questions: (i) is there a significant difference in the nuclear organization of chromosomes in H and RS cells, and (ii) can we follow the mechanisms and dynamics of chromosomal rearrangements during the transition of H to RS cells? To investigate these questions, we first carried out 3D FISH of 3D-preserved nuclei derived from H and RS cells. Using chromosome painting for chromosomes 9 (red) and 22 (green), we first studied the nuclear positions of these two chromosomes in primary human lymphocytes and in cells from patients with chronic myeloid leukemia (Figure 1A-C). As reported by others,[32] our analyses confirmed that these two chromosomes are in close vicinity in normal lymphocytes (Figure 1A). In contrast, they show
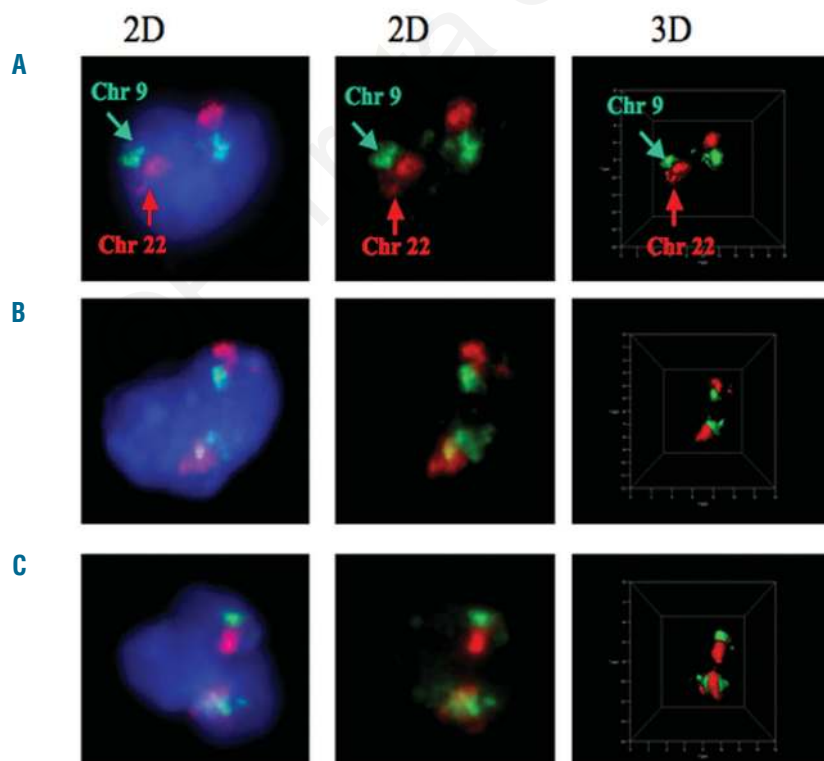

Figure 1. Two-dimensional (2D) and three-dimensional (3D) visualization of chromosome positions in patients with lymphocytes of a healthy donor and of a chronic myeloid leukemia. Chromosome 9 is labeled in green, and chromosome 22 is labeled in red. Nuclei are stained in blue (4',6-diamidino-2-phenylindole; DAPI). Each 2D image is shown with and without DAPI, 3D images are shown without DAPI. Note that chromosomes 9 and 22 are neighbors in healthy individuals, while they are juxtaposed due to the reciprocal translocation between chromosomes 9 and 22 in patients with chronic myeloid leukemia. For details, see text, and for the karyotype of chronic myeloid leukemia, see *Online Supplementary Figure S2.*

overlaps indicative of the t(9;22), characteristic of chronic myeloid leukemia (Figure 1B,C, *Online Supplementary Figure S2*). Next, we investigated the positions of these same chromosomes in H and RS cells of Hodgkin's lymphoma. We chose three common Hodgkin cell lines, HDLM-2, L-1236 and L-428, for our analysis. We have previously shown that these lines reflect the 3D telomeric organization found in Hodgkin tissues and show similar centrosome and spindle aberrations as observed in primary patients' tissues.[1]

Figure 2A illustrates the distribution of chromosomes 9 and 22 and derivate material in two representative H cell nuclei of HDLM-2 cells. The distribution of chromosome 22 (green) and 9 (red) is different in the two nuclei, with two major territories of chromosome 22 seen in the right nucleus and one cluster in the left. Chromosome 9 is found in several locations adjacent to and separate from the chromosome 22 territories. Separate color channel representations of these data are shown in *Online Supplementary Figure S3*. In contrast to H cells, RS cells exhibit greater differences in chromosome 9 and 22 numbers and show the unequal distributions of these very same chromosomes throughout each of the multi-nuclear sub-nuclei. Figure 2B illustrates these findings for a representative tri-nucleated RS cell, in which the top left nucleus contains the overwhelming content of chromosomal material, while the nuclei to the bottom left and right are poor in chromosome 9 and 22 contents.

Similar analyses were performed in L-1236 and L-428 cells. Figure 3 shows a comparison of representative nuclei of H and RS cells of L-1236. Measurements of chromosomal overlaps observed in 30 nuclei of H and RS cell in each of the Hodgkin cell lines, indicated significant increases in the number of overlaps in RS cells compared to H cells of HDLM-2 (*P*=0.030) (Figure 4) and a trend towards an increase in overlaps from H to RS cells in L-428, but not in L-1236 (*Online Supplementary Figure S3A*,B, *P*=0.11 and *P*=0.34, respectively).

We conclude that: (i) chromosomes 9 and 22 are not observed in their regular territories in Hodgkin cells irrespective of their mono- or multi-nucleated nature; (ii) the spatial distribution and number of these two chromosomes is different from nucleus to nucleus; (iii) some nuclei of RS cells are chromosome-poor containing no or very little chromosome 9 or 22 material; (iv) such nuclei can be considered 'ghost' cell nuclei;[1,9] and (v) the number of overlaps between the two chromosomes seen in interphase nuclei may vary between H and RS cells.

Rearranged chromosomes 9 and 22 in Hodgkin cells

To better understand the above findings in interphase nuclei of H and RS cells, we examined the impact of spatial disruption of chromosome 9 and 22 on genome (in)stability in metaphase spreads from the above Hodgkin cells. A minimum of 20 metaphases was analyzed in three independent experiments from HDLM-2, L-1236 and L-428. Chromosomal rearrangements involving chromosomes 9 and 22, alone or in combination, were seen in all three lines.

In the HDLM-2 line (Table 1), 47/62 metaphases (75.8%) displayed one copy of chromosome 9, and 55/62 (88.7%) of metaphases had two copies of chromosome 22. Forty-
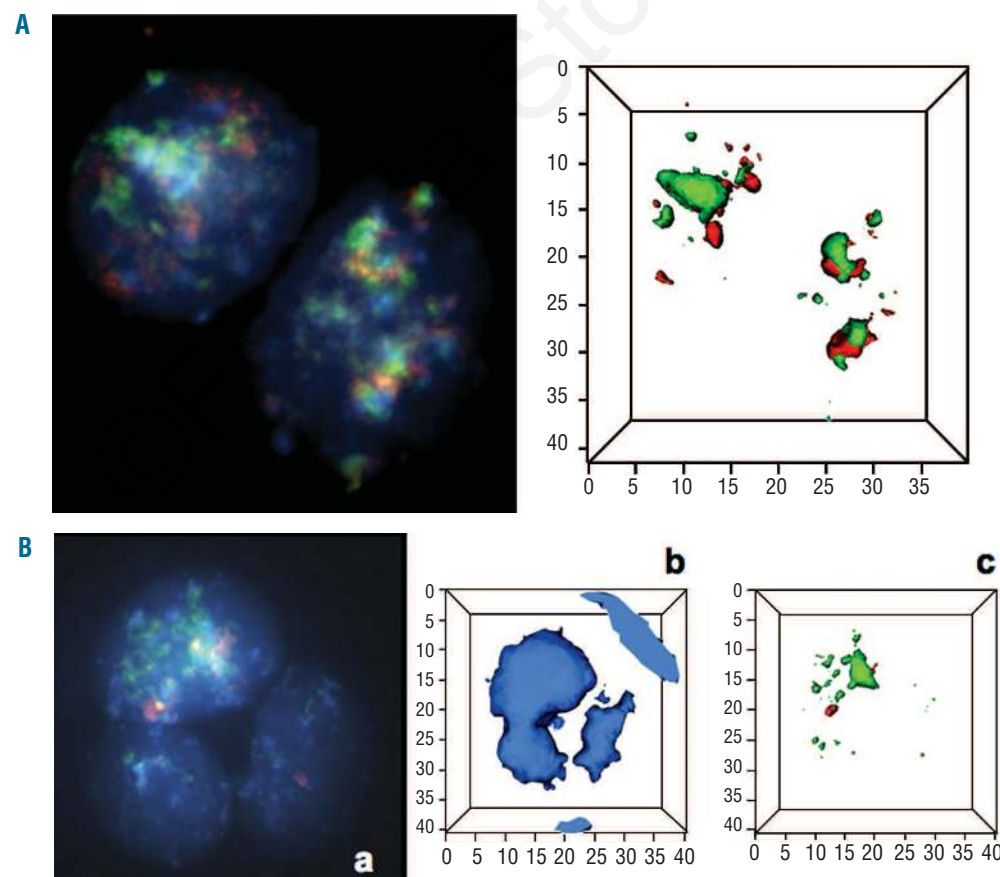

Figure 2. Interphase chromosome positions of mono-nucleated H cells of HDLM-2. (A) Chromosome painting highlights chromosomes 9 (red) and 22 (green) in two representative mono-nucleated H cells. Left image: 2D representation of the H nuclei, right image: 3D representation of these H nuclei. For clarity, the DAPI channel has been removed in this image. (B) Interphase chromosome positions of tri-nucleated RS cell of HDLM-2. Chromosome painting was carried out with chromosomes 9 (red) and 22 (green). (a) Representative 2D image of tri-nucleated RS cell. (b) DAPI channel of a) delineating the three nuclei in 3D surface mode projection. (c) Unequal 3D distribution of chromosomes 9 and 22 throughout the nuclei of the tri-nucleated RS cell. Note that most chromosome content is found in the top left nucleus, while the bottom left nucleus is significantly poorer in chromosome 9 and 22 content, and the right bottom nucleus is chromosome 9 and 22–poor ('ghost' cell).

seven of 62 (75.8%) metaphases had two translocated copies of chromosome 9, but none of chromosome 22. However all 62 metaphases (100%) had five or more fragments of chromosome 22. Every metaphase also exhibited a chromosome containing translocated pieces of both chromosomes 9 and 22, and, out of those, 43 metaphases (69.3%) displayed at least two copies of these translocations. As shown in Figure 5A-C (arrows), we identified a very characteristic chromosome that was seen in all 62 metaphases with at least one copy, containing fragments of both chromosome 9 and 22, in a 'zebra'-stripe like pattern. Since this appearance is typical of a chromosome that has undergone repeated BBF cycles, we called it the 9.22 breakage-bridge-fusion chromosome (9.22 BBFC).

L-428 (Table 1) contained 23/62 metaphases (37%) with two copies and 29/62 metaphases (46.8%) with three copies of chromosome 9. Forty of the metaphases (64.5%) contained two copies of a translocated chromosome 9. Thirty-two of the metaphases (51.6%) displayed three copies of chromosome 22. Both chromosome 9 and 22 translocated with a third chromosome in all but two metaphases representing 96.8% of the cases, and 40 of those contained two copies of these two-way translocation chromosomes (66.6%). Unlike the chromosome 9 translocations recorded, chromosome 22 showed multiple fragments, and was translocated to various chromosomes. Insertions of chromosomes 9 and 22 were also noted. *Online Supplementary Figure S5* illustrates one representative
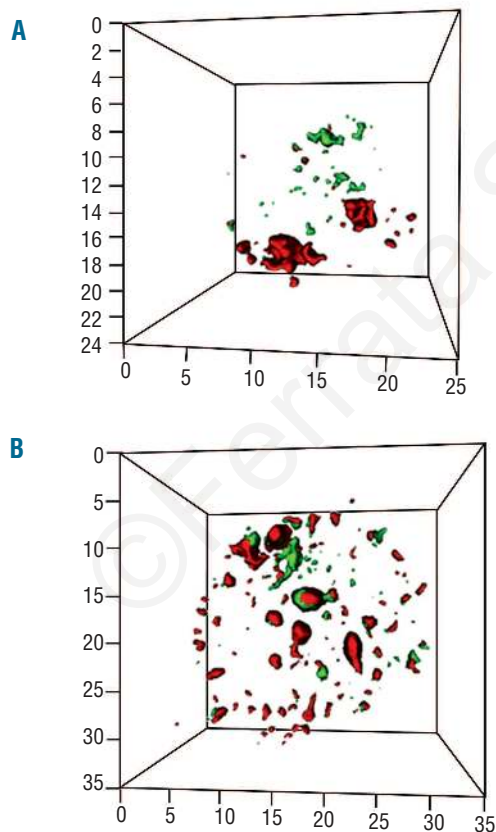
example of chromosomes 9 and 22 in L-428.

L-1236 (Table 1) contained 39/62 metaphases (62.9%) with two copies of chromosome 9, and 42 metaphases (67.7%) with one copy of chromosome 22. There were 34 metaphases (54.8%) with one copy of a chromosome 9 translocation, while chromosome 22 was involved in translocations in 29/62 metaphases (46.8%). Like L-428 (Table 1 and *Online Supplementary Figure S6*), L-1236 also showed the presence of fragments derived from chromo-
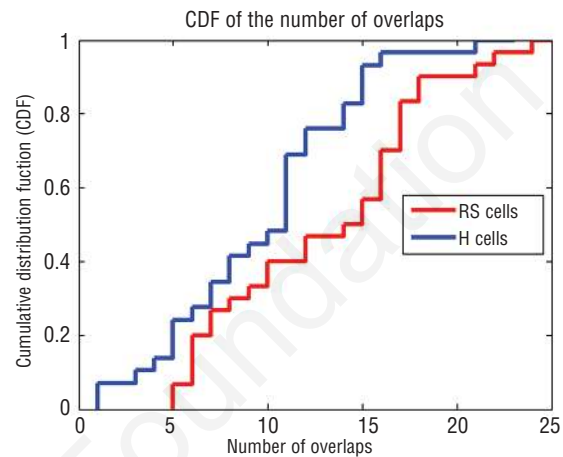

Figure 4. Cumulative distribution functions of the number of overlaps for chromosomes 9 and 22. The curves illustrate the distribution of chromosomes 9 and 22 for HDLM-2 (P=0.03). The P values are obtained by the Kolmogorov-Smirnov test applied to the data shown in the figures. The red line illustrates the overlaps of chromosomes 9 and 22 in RS cells, while the blue line show this comparison for H cells. Thirty nuclei were measured each for H and RS cells.
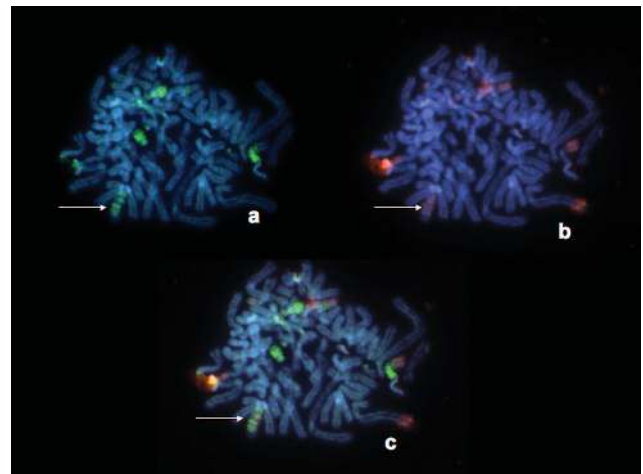

Figure 3. Interphase chromosome positions of H and RS cells of L-1236. (A) 3D image of the nuclear distribution of chromosomes 9 (red) and 22 (green) in a representative H cell of L-1236. (B) 3D nuclear distribution of chromosomes 9 and 22 in a RS cell of L-1236.

Figure 5. Metaphase spreads illustrate multiple rearrangements involving chromosomes 9 and 22. Chromosome painting with chromosomes 9 (red) and green (22) in HDLM-2. (a) Hybridization signals detected with chromosome 22 (green) on DAPI-counterstained chromosomes of HDLM-2. The arrow points to a chromosome with multiple bands of chromosome 22. (b) Hybridization signals detected with chromosome 9 (red) on the identical DAPI-counterstained chromosomes shown in (a). The arrow points to the identical chromosome shown in (a) that also carries red bands indicating chromosome 9 origin. (c) Overlay of images (a) and (b). The arrow points to the 'zebra'-type chromosome that carries chromosome 9 and 22 material due to breakage-bridge-fusion (BBF) cycles. For more details, see text. Note additional rearrangements involving chromosomes 9 and 22. Table 1 summarizes the overall involvement of chromosomes 9 and 22 in HDLM-2, L-428 and L-1236.

some 22, however there were five or fewer fragments per metaphase (Table 1).

We conclude that Hodgkin cells show multiple rearrangements involving chromosomes 9 and 22. The aberrations include numerical and structural changes. The latter involve single, double or multiple unbalanced translocation events characteristic of BBF cycles.

Spectral karyotyping reveals extensive and complex chromosomal rearrangements in Hodgkin cells

Using the same metaphase preparations as analyzed in the metaphase FISH for chromosomes 9 and 22, we examined overall chromosomal changes in these three cell lines using SKY. Twenty metaphases for each cell line were imaged and analyzed using Case Data Manager and

Table 1. Summary of data obtained after chromosome painting of Hodgkin's interphase nuclei with chromosomes 9 and 22.

	chr 9	chr 9 trans	chr 9 fragment	chr9 and 22 together	chr 22	chr 22 trans	chr 22 fragment	BBF chr
HDLM-2								
	47 have 1 copy	10 have 1 copy	62 have 0 copies	16 have 1 copy	7 have 1 copy	62 have 0 copies	62 have 5+ copies	59 have 1 copy
	14 have 2 copies	47 have 2 copies		43 have 2 copies	55 have 2 copies			3 have 2 copies
	1 has 3 copies	2 have 3 copies		3 have 3 copies				
		1 has 4 copies						
L-1236								
	14 have 1 copy	4 have 0 copies	3 have 1 copy	62 have 0 copies	4 have 0 copies	4 have 0 copies	3 have 0 copies	62 have 0 copies
	39 have 2 copies	34 have 1 copy	1 has 3 copies		42 have 1 copy	29 have 1 copy	2 have 1 copy	
	8 have 3 copies	16 have 2 copies			14 have 2 copies	16 have 2 copies	8 have 2 copies	
	1 has 7 copies	4 have 3 copies			2 have 3 copies	7 have 3 copies	12 have 3 copies	
		2 have 4 copies			0 have 4 copies	4 have 4 copies	12 have 4 copies	
		1 has 5 copies			0 have 5 copies	2 have 5 copies	25 have 5+ copies	
		1 has 6 copies						
L-428								
	4 have 1 copy	4 have 1 copy	62 have 0 copies	2 have 0 copies	1 have 1 copy	1 has 1 copy	4 have 0 copies	62 have 0 copies
	23 have 2 copies	23 have 2 copies		16 have 1 copy	7 have 2 copies	1 has 2 copies	0 have 1 copy	
	29 have 3 copies	29 have 3 copies		40 have 2 copies	32 have 3 copies	1 has 7 copies	58 have 5+ copies	
	4 have 4 copies	4 have 4 copies		3 have 3 copies	13 have 4 copies			
	2 have 5 copies	2 have 5 copies		1 has 5 copies	4 have 5+ copies			
	1 has 6 copies	1 has 6 copies						

Results are shown for HDLM-2, L-1236, and L-428 cells.
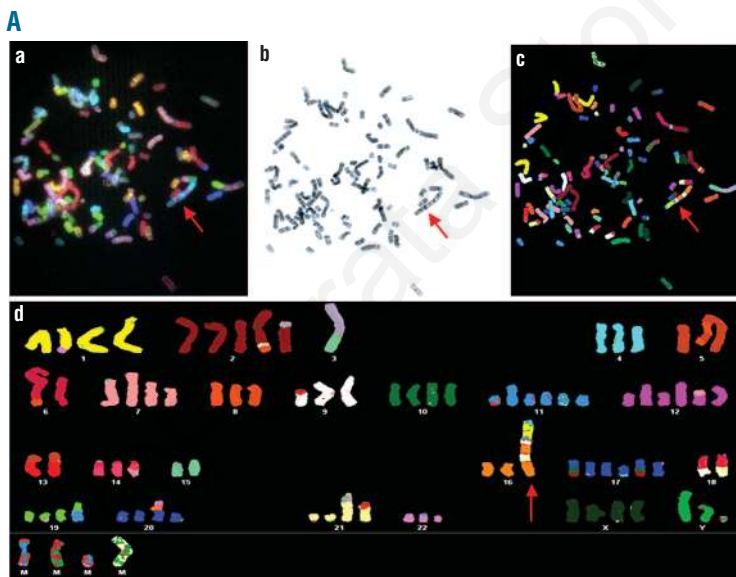
A

B

Figure 6. (A) Spectral karyotyping (SKY) of L-428. Representative figure illustrating complex chromosomal rearrangements indicative of BBF cycles, unequal chromosome segregation and centrosome duplication defects. (a) is the raw spectral image, (b) is the inverted DAPI image, (c) is the pseudo-color image and finally (d) is the karyotype table, which shows the classification of chromosomes. An arrow points to the most prominent BBF chromosome ('zebra'-type). *Online Supplementary Table S1* summarizes all numerical and structural chromosomal changes detected. *Online Supplementary Figure S5* shows representative SKY data for HDLM-2 and L-1236. (B) Super resolution imaging (3D-SIM) of H and RS cells. 3D-fixed nuclei of HDLM-2 were imaged using 3D-SIM. (a) Intra-nuclear bridges between RS cell nuclei [arrows and insert (b)]; (c) a chromosome that forms a bridge between two RS cells (see arrow and insert).
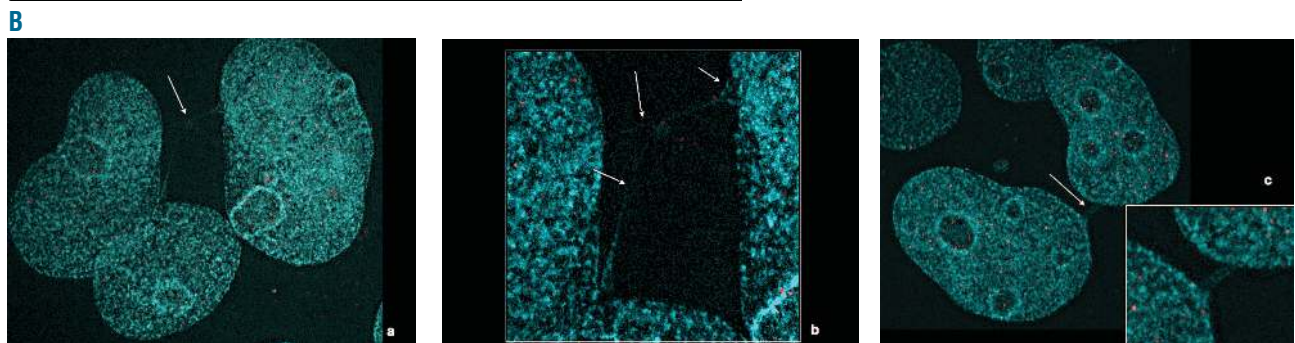
SKY View software.

Every metaphase analyzed for all three Hodgkin lines, HDLM-2, L-428, and L-1236, had some form of chromosomal rearrangement ($P<0.0001$). Representative figures illustrate the findings for all three lines (Figure 6A, and *Online Supplementary Figure S6*). Figure 6A (arrow) shows the presence of a 'zebra'-type BBF chromosome having undergone multiple BBF cycles, similar to the BBF chromosome (9.22 BBFC) observed in HDLM-2 (Figure 5A-C), but involving different chromosome partners.

The pairs of chromosomes repeatedly involved in translocation events in all three cell lines and at a frequency of ten or more times were also analyzed (Table 2). Chromosomes 13 and 16, 13 and 5, 14 and 21, 15 and 20, 15 and 22, 15 and 8, 5 and 4, 6 and 22, 7 and 3, and 8 and 2 all had *P* values of less than 0.0001. Rearrangements involving pairs of chromosomes, such as chromosomes 10 and 17 ($P=0.0002$), 12 and 22 ($P=0.0411$), 12 and 4 ($P=0.001$), 11 and 13 ($P=0.001$), 11 and 16 ($P=0.0029$), 5 and 21 ($P=0.0016$), 5 and 22 ($P=0.0123$), and 2 and 10 ($P=0.0534$), were all significant as well. Chromosome 9 and 22 aberrations, as described above, were confirmed (*Online Supplementary Table S1*).

To examine the progression from H to RS cells, we analyzed the complexity of chromosomal rearrangements between H and RS cells of the same cell lines (*Online Supplementary Table S1*). *Online Supplementary Table S1* highlights common dynamic rearrangements in H and RS

Table 2. Translocation summary and statistical significance of translocations observed.

Translocations	*P* value
Chromosomes 1 and 11	0.1864
Chromosomes 10 and 17	0.0002
Chromosomes 12 and 22	0.0411
Chromosomes 12 and 4	0.001
Chromosomes 11 and 13	0.0011
Chromosomes 13 and 16	<0.0001
Chromosomes 11 and 16	0.0029
Chromosomes 13 and 5	<0.0001
Chromosomes 14 and 21	<0.0001
Chromosomes 15 and 20	<0.0001
Chromosomes 15 and 22	<0.0001
Chromosomes 15 and 8	<0.0001
Chromosomes 1 and 7	0.0602
Chromosomes 5 and 21	0.0016
Chromosomes 5 and 22	0.0123
Chromosomes 2 and 10	0.0534
Chromosomes 3 and 21	0.8644
Chromosomes 5 and 4	<0.0001
Chromosomes 5 and 1	0.6787
Chromosomes 5 and 6	0.7053
Chromosomes 9 and 21	0.359
Chromosomes 6 and 22	<0.0001
Chromosomes 7 and 3	<0.0001
Chromosomes 8 and 2	<0.0001

SKY data are shown for chromosomes involved more than ten times in translocations in HDLM-2, L-1236 and L-428 (P values according to Fisher's exact test).

cells of HDLM-2 (highlighted in red and green). RS cells show additional chromosomal changes that exist in a less complicated form in H cells. For example, t(1;17) is found in H cells, and becomes a three- or four-way translocation in RS cells t(1;17;13;18) or t(1;17;19;18) (*Online Supplementary Table S1*; red) and t(2;21) becomes t(2;21;6;17) (*Online Supplementary Table S1*; green).

Telomere dysfunction in Hodgkin's lymphoma[1] was confirmed and included telomere-free ends and interstitial telomere signals in many chromosomes of all metaphases examined for all cell lines (*Online Supplementary Table S2*).

We conclude that H and RS cells have complex karyotypes that reflect their disrupted nuclear chromosomal organization. RS cells continue to acquire additional changes and become overloaded with multiple rearranged and fused chromosomes. They demonstrate the karyotypic evolution that began in H cells, possibly already in small circulating precursors, reaching an end-stage of complexity in RS cells.

Super resolution imaging reveals nuclear remodeling and frequent breakage-bridge-fusion cycles in Reed-Sternberg cells

To validate the above conclusions, we carried out 3D-SIM and established that H cells have a more uniform nuclear architecture than bi- to multi-nucleated RS cells (Figure 6B, and *Online Supplementary Figure S7*). H cells rarely showed inter-nuclear bridges indicative of ongoing BBF cycles (*Online Supplementary Figure S7A,B*). In contrast, RS nuclei are commonly linked to each other through single or multiple inter-nuclear bridges, consisting of stretched DNA fibers and/or of individual chromosomes (Figure 6B, a-c). Thus, BBF cycles are frequent in RS cells and lead to their complex karyotypes and complex karyotype evolution.

Discussion

Disruption of nuclear architecture in Hodgkin's lymphoma

The nucleus and its architecture are key to proper cell function, including replication and transcription and maintenance of genomic stability.[33-35] The strongest functional evidence linking chromosome architecture and cellular function was recently demonstrated in rod cell nuclei.[36] The authors convincingly demonstrated regular and inverted chromosomal architecture in rod cells, and this architecture was associated with diurnal and nocturnal vision. Chromosomes are thus organized in a non-random manner to assure cellular function. Any change to this organization will necessarily have an impact on the function of the affected cell.

Hodgkin cells show successively increasing disruption of their nuclear architecture starting with H cells and dynamically progressing to RS cells. Chromosomal positions in H and RS cells were examined in three Hodgkin cell lines and all displayed alterations from the 3D nuclear order of the same chromosomes in normal human B cells. In addition, the RS nuclear chromosome distribution was uneven and the numbers of chromosomes found in each sub-nucleus differed as demonstrated for chromosomes 9 and 22 and validated by SKY. This study is, to the best of our knowledge, the first to demonstrate the progressive disruption of nuclear chromosomal order in Hodgkin's lymphoma.

Complex chromosome dynamics during the transition of Hodgkin cells to Reed-Sternberg cells

We detected aberrations from the normal positioning of chromosomes in H cells, and these nuclear chromosome positions were reflected by chromosomal rearrangements. The latter were studied by chromosome painting for chromosomes 9 and 22 and followed up for all chromosomes using SKY. The findings were complementary: H cells possess unstable genomes and show cell-to-cell variations.

As H cells transition to RS cells, the situation becomes more complex as some nuclei show unequal chromosome distribution and others become 'ghost' nuclei, devoid of the normal DNA content. This refers to both telomeres[1,9] and chromosomes (this study). Chromosomes 9 and 22 are indicators of this situation. These two chromosomes are not commonly found in 'ghost' nuclei, and therefore such ghost cells have to be considered chromosome-poor. In contrast, some of the RS cell nuclei are chromosome-rich and contain multiple sets of these chromosomes. Thus, RS cells were subject to the dynamic processes that occurred during the transition from H to RS cell, including aberrant centrosome duplication, multiple spindles and increasing levels of aneuploidy. In addition, due to telomere dysfunction brought about by critically short telomeres and telomere uncapping,[1] telomeric end-to-end fusions create dicentric chromosomes that break at anaphase and generate ongoing cycles of BBF. The latter were observed in each metaphase plate and highlighted by 3D-SIM (Figure 6B). Varying BBF partners joined into this process when H cells became RS cells (Figures 5 and 6A, and *Online Supplementary Table S1*).

Genomic instability in Hodgkin cells

Genomic instability is a dynamic process that enables the cell population to evolve in different ways depending on selective pressures. The genetic heterogeneity found in H cells and recapitulated at higher complexity in RS cells suggests that the H cell acquires additional genetic hits during transition to the RS cell stage. These include telomere-mediated BBF cycles with unbalanced translocations and multiple rounds of BBF generating BBF (zebra) chromosomes that were created by repeated breakage and fusions between the one, two or multiple chromosomes.

The question arises how much genomic instability cells require to adapt to their tumorigenic environment and how much instability they can take before they reach their own replicative end-points when aberrations and fusions become a hindrance to further cell divisions. Work in tumor models suggested that too high a level of genomic instability limited tumor growth.[37] Recent data from our group suggest that early *ex vivo* Epstein-Barr virus-infected human B lymphocytes display genomic instability and show dynamic karyotype evolution.[10,38] Taken together, we propose that H cells are tumor cells with altered nuclear architecture and resulting chromosomal rearrangements at a level that still supports tumor growth. In contrast, RS cells 'struggle' to keep dividing; not only is their nuclear architecture further disrupted, not only do they contain 'ghost cell nuclei' with little telomeric material[1,9] and low levels of chromosomal material, they also have an uneven distribution of genetic material within each of their sub-nuclei (Figure 2B). Chromosomal territories are disrupted, chromosomal rearrangements continue to occur, aneuploidy increases and genetic diversity within a single RS cell (referring to each of its sub-nuclei) is enhanced with each attempt to divide. This appears to be a scenario that is not likely to generate new and aggressively proliferating tumor cells, but huge multi-nucleated giant cells that, by continuously increasing their karyotypic evolution, run out of options for proper cell division.

Clinical implications

There is now ample evidence that RS cells are producers of an impressive number of cytokines, chemokines and surface receptors, allowing them to attract a high number of non-malignant reactive cells such as Th2 lymphocytes, eosinophils and macrophages, which in return stimulate H- and RS-cell growth and additional cytokine production through activation of nuclear factor-κB.[6,39,40] Moreover, H and RS cells sustain their own growth by an autocrine interleukin-13 loop.[41] In this context the RS cells, though end-stage tumor cells,[1,9] stimulate mitosis of their direct precursors, the mononuclear H cells, and probably also the recruitment of small circulating early precursors.[5] In this scenario progression of Hodgkin's lymphoma is fueled by a permanent inflammatory stimulus.[42] Indeed, suppression of inflammatory stimulus by acetylsalicylic acid significantly decreases the risk of getting Hodgkin's lymphoma.[43] Thus, interruption of this vicious circle through neutralization of its key player, the RS cell, is expected to shut down proliferation of H and RS cells as well as associated B-symptoms such as cytokine-induced fever and sweats. Since terminal RS cells are characterized by disturbed nuclear architecture, disruption of the shelterin complex, aberrant mitotic spindle formation and erosion of telomeres[1,9,10] facilitating the formation of giant BBF (zebra) chromosomes, innovative therapeutic approaches should focus on these newly identified targets.

Authorship and Disclosures

References

1. Knecht H, Sawan B, Lichtensztejn D, Lemieux B, Wellinger RJ, et al. The 3D nuclear organization of telomeres marks the transition from Hodgkin to Reed-Sternberg cells. Leukemia. 2009;23(3):565-73.

2. Küppers R. The biology of Hodgkin's lymphoma. Nat Rev Cancer. 2009;9(1):15-27.

3. Pallesen G, Hamilton-Dutoit SJ, Rowe M, Young LS. Expression of Epstein-Barr virus latent gene products in tumour cells of Hodgkin's disease. Lancet.1991;337(8737): 320-2.

4. Knecht H, Bachmann E, Brousset P, Sandvej K, Nadal D, Bachmann F, et al. Deletions within the LMP1 oncogene of Epstein-Barr virus are clustered in Hodgkin's disease and identical to those observed in nasopharyngeal carcinoma. Blood. 1993;82(10):2937-42.

5. Jones RJ, Gocke CD, Kasamon YL, Miller CB, Perkins B, Barber JP, et al. Circulating clonotypic B cells in classical Hodgkin lymphoma. Blood. 2009;113(23):5920-6.

6. Skinnider BF, Mak TW. The role of cytokines in classical Hodgkin lymphoma. Blood. 2002;99(12):4283-97.

7. Kuruvilla J. Standard therapy of advanced Hodgkin lymphoma. Hematology Am Soc Hematol Educ Program. 2009:497-506.

8. Mai S, Imreh S. Non-random genomic instability in cancer: a fact, not an illusion. Semin Cancer Biol. 2007;17(1):1-4.

9. Knecht H, Sawan B, Lichtensztejn Z, Lichtensztejn D, Mai S. 3D Telomere FISH defines LMP1-expressing Reed-Sternberg cells as end-stage cells with telomere-poor 'ghost' nuclei and very short telomeres. Lab Invest. 2010; 90(4):611-9.

10. Mai S. Initiation of telomere-mediated chromosomal rearrangements in cancer. J Cell Biochem. 2010; 109(6):1095-102.

11. Müller HJ. The remaking of chromosomes. Collecting Net. 1938;13:181-98.

12. McClintock B. The stability of broken ends of chromosomes in Zea mays. Genetics. 1941;26(2):234-82.

13. McClintock B. The fusion of broken ends of chromosomes following nuclear fusion. Proc Natl Acad Sci USA. 1942;28:458–63.

14. Selvarajah S, Yoshimoto M, Park PC, Maire G, Paderova J, Bayani J, et al. The breakage-fusion-bridge (BFB) cycle as a mechanism for generating genetic heterogeneity in osteosarcoma. Chromosoma. 2006;115(6): 459-67.

15. Vukovic B, Park PC, Al-Maghrabi J, Beheshti B, Sweet J, Evans A, et al. Evidence of multifocality of telomere erosion in high-grade prostatic intraepithelial neoplasia (HPIN) and concurrent carcinoma. Oncogene 2003;22(13):1978-87.

16. Vukovic B, Beheshti B, Park P, Lim G, Bayani J, Zielenska M, et al. Correlating breakage-fusion-bridge events with the overall chromosomal instability and in vitro karyotype evolution in prostate cancer. Cytogenet Genome Res. 2007;116(1-2):1-11.

17. Meeker AK, Hicks JL, Gabrielson E, Strauss WM, De Marzo AM, Argani P. Telomere shortening occurs in subsets of normal breast epithelium as well as in situ and invasive carcinoma. Am J Pathol. 2004; 164(3):925-35.

18. Stewénius Y, Gorunova L, Jonson T, Larsson N, Höglund M, Mandahl N, et al. Structural and numerical chromosome changes in colon cancer develop through telomere-mediated anaphase bridges, not through mitotic multipolarity. Proc Natl Acad Sci USA. 2005;102(15):5541-6.

19. DePinho RA, Polyak K. Cancer chromosomes in crisis. Nat Genet. 2004;36(9):932-4.

20. Lansdorp PM. Telomeres and disease. EMBO J. 2009;28(17):2532-40.

21. Murnane JP, Sabatier L. Chromosome rearrangements resulting from telomere dysfunction and their role in cancer. Bioessays. 2004;26(11):1164-74.

22. Lingle WL, Lukasiewicz K, Salisbury JL. Deregulation of the centrosome cycle and the origin of chromosomal instability in cancer. Adv Exp Med Biol. 2005;570:393-421.

23. Duensing A, Spardy N, Chatterjee P, Zheng L, Parry J, Cuevas R, et al. Centrosome overduplication, chromosomal instability, and human papillomavirus oncoproteins. Environ Mol Mutagen. 2009;50(8):741-7.

24. Pihan GA, Purohit A, Wallace J, Knecht H, Woda B, Quesenberry P, et al. Centrosome defects and genetic instability in malignant tumors. Cancer Res. 1998;58(17):3974-85.

25. MacLeod RA, Spitzer D, Bar-Am I, Sylvester JE, Kaufmann M, Wernich A, et al. Karyotypic dissection of Hodgkin's disease cell lines reveals ectopic subtelomeres and ribosomal DNA at sites of multiple jumping translocations and genomic amplification. Leukemia. 2000;14(10):1803-14.

26. Martin-Subero JI, Knippschild U, Harder L, Barth TF, Riemke J, Grohmann S, et al. Segmental chromosomal aberrations and centrosome amplifications: pathogenetic mechanisms in Hodgkin and Reed-Sternberg cells of classical Hodgkin's lymphoma. Leukemia. 2003;17(11):2214-9.

27. Guffei A, Lichtensztejn Z, Gonçalves Dos Santos Silva A, Louis SF, Caporali A, Mai S. c-Myc-dependent formation of Robertsonian translocation chromosomes in mouse cells. Neoplasia. 2007;9(7):578-88.

28. Beatty B, Mai S, Squire J (Eds). (2002) FISH: A Practical Approach. Oxford University Press.

29. Schaefer LH, Schuster D, Herz H. Generalized approach for accelerated maximum likelihood based image restoration applied to three-dimensional fluorescence microscopy. J Microsc. 2001;204(Pt 2):99-107.

30. Ridler TW, Calvard S. Picture thresholding using an iterative selection method. IEEE Trans Syst Man Cybern SMC-1978;8: 630-2.

31. Louis SF, Vermolen BJ, Garini Y, Young IT, Guffei A, Lichtensztejn Z, et al. c-Myc induces chromosomal rearrangements through telomere and chromosome remodeling in the interphase nucleus. Proc Natl Acad Sci USA. 2005;102(27):9613-8.

32. Kozubek S, Lukásová E, Marecková A, Skalníková M, Kozubek M, Bártová E, et al. The topological organization of chromosomes 9 and 22 in cell nuclei has a determinative role in the induction of t(9,22) translocations and in the pathogenesis of t(9,22) leukemias. Chromosoma. 1999;108 (7):426-35.

33. Grasser F, Neusser M, Fiegler H, Thormeyer T, Cremer M, Carter NP, et al. Replication-timing-correlated spatial chromatin arrangements in cancer and in primate interphase nuclei. J Cell Sci. 2008;121(Pt 11):1876-86.

34. Lanctôt C, Cheutin T, Cremer M, Cavalli G, Cremer T. Dynamic genome architecture in the nuclear space: regulation of gene expression in three dimensions. Nat Rev Genet. 2007;8(2):104-15.

35. Cremer T, Cremer M, Dietzel S, Müller S, Solovei I, Fakan S. Chromosome territories-a functional nuclear landscape. Curr Opin Cell Biol. 2006;18(3):307-16.

36. Solovei I, Kreysing M, Lanctôt C, Kösem S, Peichl L, Cremer T, et al. Nuclear architecture of rod photoreceptor cells adapts to vision in mammalian evolution. Cell. 2009;137(2):356-68.

37. Weaver BA, Cleveland DW. The aneuploidy paradox in cell growth and tumorigenesis. Cancer Cell. 2008;14(6):431-3.

38. Lacoste S, Wiechec E, Dos Santos Silva AG, Guffei A, Williams G,Lowbeer M, et al. Chromosomal rearrangements after ex vivo Epstein-Barr virus (EBV) infection of human B cells. Oncogene. 2010;29(4):503-15.

39. Maggio EM, Van den Berg A, Visser L, Diepstra A, Kluiver J, Emmens R, et al. Common and differential chemokine expression patterns in RS cells of NLP, EBV positive and negative classical Hodgkin lymphomas. Int J Cancer. 2002;99(5):665-72.

40. Khan G. Epstein-Barr virus, cytokines, and inflammation: a cocktail for the pathogenesis of Hodgkin's lymphoma? Exp Hematol. 2006;34(4):399-406.

41. Kapp U, Yeh WC, Patterson B, Elia AJ, Kägi D, Ho A, et al. Interleukin 13 is secreted by and stimulates the growth of Hodgkin and Reed-Sternberg cells. J Exp Med. 1999;189 (12):1939-46.

42. Pikarsky E, Porat RM, Stein I, Abramovitch R, Amit S, Kasem S, et al. NF-kappaB functions as a tumour promoter in inflammation-associated cancer. Nature. 2004;431 (7007):461-6.

43. Chang ET, Zheng T, Weir EG, Borowitz M, Mann RB, Spiegelman D, et al. Aspirin and the risk of Hodgkin's lymphoma in a population-based case-control study. J Natl Cancer Inst. 2004;96(4):305-15.